Size and shape effect on the photocatalytic efficiency of TiO2 brookite

Stéphanie Pigeot-Remy, Damia Gregori, Roumayssaa Hazime, Alexandre Hérissan, Chantal Guillard, Corinne Ferronato, Sophie Cassaignon, Christophe Colbeau-Justin, Olivier Durupthy

▶ **To cite this version:**

Stéphanie Pigeot-Remy, Damia Gregori, Roumayssaa Hazime, Alexandre Hérissan, Chantal Guillard, et al.. Size and shape effect on the photocatalytic efficiency of TiO2 brookite. Journal of Materials Science, 2019, 54 (2), pp.1213-1225. 10.1007/s10853-018-2924-x . hal-01968937

HAL Id: hal-01968937
https://hal.science/hal-01968937

Submitted on 29 Nov 2022

HAL is a multi-disciplinary open access archive for the deposit and dissemination of scientific research documents, whether they are published or not. The documents may come from teaching and research institutions in France or abroad, or from public or private research centers.

L'archive ouverte pluridisciplinaire **HAL**, est destinée au dépôt et à la diffusion de documents scientifiques de niveau recherche, publiés ou non, émanant des établissements d'enseignement et de recherche français ou étrangers, des laboratoires publics ou privés.

Distributed under a Creative Commons Attribution 4.0 International License

Size and shape effect on the photocatalytic efficiency of TiO_2 brookite

Stephanie Pigeot-Rémy[1], Damia Gregori[2], Roumayssaa Hazime[2], Alexandre Hérissan[3], Chantal Guillard[2], Corinne Ferronato[2], Sophie Cassaignon[1], Christophe Colbeau-Justin[3], and Olivier Durupthy[1,*]

[1] *Sorbonne Université, CNRS, Collège de France, Laboratoire de Chimie de la Matière Condensée de Paris (LCMCP), 4 place Jussieu, 75005 Paris, France*

[2] *Univ Claude Bernard Lyon 1, Univ Lyon, IRCELYON, CNRS, UMR 5256, 2 Av Albert Einstein, 69626 Villeurbanne, France*

[3] *Laboratoire de Chimie Physique, CNRS UMR8000, Université Paris-Saclay, Univ Paris-Sud, 91405 Orsay, France*

ABSTRACT

Thanks to aqueous sol–gel chemistry, it is now possible to prepare several phase pure TiO_2 brookite colloidal systems that significantly differ on nanoparticles size and shape. This TiO_2 polymorph is more difficult to be obtained as phase pure material than anatase or rutile. Here we have prepared a set of four different sol–gel brookite syntheses with particles size ranging from 10 to 500 nm and significantly different morphologies as demonstrated by X-ray diffraction, Raman spectroscopy, and transmission electron microscopy. We have studied their photocatalytic activities in aqueous solution on phenol and formic acid. The brookite sample with higher specific surface displays better activity for both pollutants abatement than anatase and rutile reference samples and very close to the TiO_2 P25 commercial reference. Additional experimental characterization of photogenerated charge carriers and their lifetime is performed using time-resolved microwave conductivity. We could then explain why another efficient brookite material is able to compensate a significantly lower specific surface with a higher photon conversion rate. This study involving a broad set of pure phase brookite samples brings back that phase into the TiO_2 polymorphs race for light-enhanced applications. It confirms that size/shape–activity correlation already observed for the anatase polymorph is also valid for the brookite phase.

Introduction

Titanium dioxide, TiO_2, is a key material already widely used for a wide span of industrial applications such as pigment in paper industry, food additive (E171), UV blocker, catalytic support, photocatalyst, and electrochromic material, and is also extensively studied at lower technology readiness level (TRL) as oxygen sensor, lithium-ion battery electrode, or dye-sensitized solar cell (DSSC)

Address correspondence to E-mail: olivier.durupthy@sorbonne-universite.fr

https://doi.org/10.1007/s10853-018-2924-x

electrode [1–8]. In most of applications, that oxide is used as nanoparticles or as nanostructured materials in order to provide an important interface.

With the same chemical composition, three polymorphs can be obtained depending on preparation mode. This polymorphism impacts noticeably toward the above-quoted applications. Indeed, if selected physical properties are quite close such as a band gap in the 3.0–3.2 eV range, others distinguish a structure from the others: For instance, rutile presents a direct bandgap, while it is indirect in anatase and brookite [9, 10]. Other bulk properties (charge carrier mobility, flat band potential position, etc.) or surface composition variation also change with structure [11–15]. Consequently, anatase and rutile structures are said to be better candidates for some applications. For instance, thanks to a better mobility of charge carriers and good sub-surface charge-trapping sites, anatase is known to be a better photovoltaic and photocatalytic material than rutile [9, 16]. However, several studies have shown that photocatalytic efficiency also strongly depends on size, shape, surface state, and dispersion state of the particles used. This was well documented on the anatase phase and less extensively for brookite [10, 11, 17–25]. When a clearly defined pollution case is tackled, the best photocatalyst is of course the material that is able to degrade, in the defined conditions, a maximum of the targeted pollutant into non noxious products. Otherwise, a good photocatalytic material should be able to degrade reasonably rapidly, in model conditions, different kinds of model pollutants. Ideally, a total mineralization is foreseen. At least, first decomposition products should be less noxious than the initial pollutant.

It is possible to find studies on selected pollutants where brookite materials are found to be more active than anatase ones or even than the TiO_2 P25 reference photocatalyst [26–32]. For Cr(VI) reduction reaction for instance, brookite seems more photoactive than rutile or anatase [33]. However, up to now, there is no benchmark photocatalytic study where several brookite materials prepared via significantly different methods are compared to established references of anatase and commercial photocatalyst on well-designed photocatalytic tests.

In this context, we present in this study the syntheses of pure brookite nanoparticles with four different morphologies. The different samples were fully characterized in order to ensure the purity of the TiO_2 phase and to describe precisely the characteristics of the nanoparticles. Their photocatalytic activity was evaluated on two model pollutants in water: phenol and formic acid under very carefully defined conditions [34–36]. The activity was compared to that of Evonik P25 anatase–rutile mixed phase as well as two pure TiO_2 anatase and rutile references previously selected for good activity on the same pollutants. The photogeneration of electrons and holes in the different materials and their mobility in the nanoparticles is also studied using time-resolved microwave conductivity (TRMC). The activity of the different brookite samples is then discussed and trends are defined to determine the key parameters of a good photocatalytic activity in that phase.

Materials and methods

Particles synthesis

As reviewed more in details elsewhere [10, 32], the preparation of pure brookite particles can be done through different hydrothermal experimental conditions but each time with a rather finely tuned set of parameters. For instance, a recently published article reports the formation of brookite nanorods from a titanium–glycolate complex in the presence of lysine after 24 h of aging at 200 °C [37]. Changing the titanium source, the amino acid of the temperature would yield impure brookite or even no brookite at all. The orientation of inorganic polymerization to the brookite structure is said to be due to a specific inorganic molecular precursor ($[Ti(OH)_2Cl_2(OH_2)_2]^0$ in Pottier et al [38].) or a polymetallic complex such as the titanium peroxoglycolate complex [39]. In other synthetic conditions, a first condensed phase, usually titanates, is formed, and the prolonged hydrothermal treatment induces a phase transformation to the brookite phase [40]. From the different experimental conditions, the final brookite particles maintain the morphology of the pristine condensed phase or may grow differently depending on the molecular precursor. That is why it is possible to vary brookite particles size and shape by changing drastically the synthetic methods (schematized in Fig. 1).

Hydrothermal evolution of lactate complex of Ti(IV) with urea (B-lactate) TiO_2 brookite particles were obtained through the hydrothermal evolution of a titanolactate complex prepared in the presence of

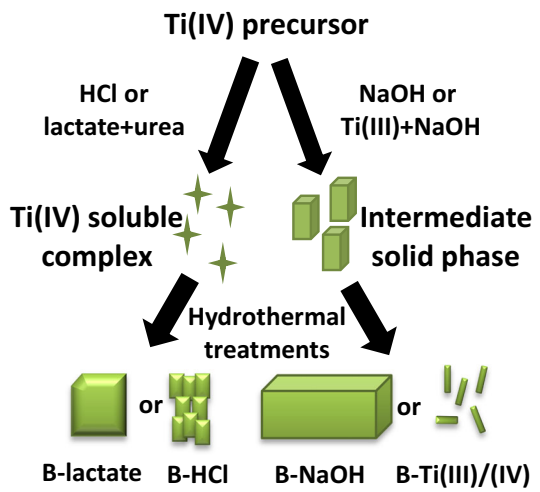

Figure 1 Schematic diagram for the formation of the different brookite samples.

urea as adapted from another group [26]. First, 60 mL of water was cooled down in an ice bath and 1.65 mL of $TiCl_4$ was added dropwise under vigorous magnetic stirring. Then 5.0 g of urea and 5.0 mL of a 60 wt % solution of sodium lactate were added under magnetic steering. Finally, the solution was transferred in autoclaves (10 mL in a 15 mL Teflon lined autoclave) and heated in a stove at 200 °C for 24 h.

Hydrothermal evolution of titanates in alkaline medium (B-NaOH) TiO_2 brookite particles were obtained through the hydrothermal evolution of a titanate precipitate initially prepared in alkaline conditions. First, 1.1 mL of $TiCl_4$ was added dropwise in few milliliters of water cooled down in an ice bath. Then the pH of the stirred solution was progressively set to 12.0 using few milliliters of a concentrated sodium hydroxide solution (10 mol L^{-1}), and the total volume of the solution was adjusted to 100 mL with water. Finally the solution was transferred in autoclaves (10 mL in a 15 mL Teflon lined autoclave) and heated in an oven at 200 °C for 24 h.

Thermohydrolysis of $TiCl_4$ in acidic medium (B-HCl) TiO_2 brookite particles were obtained through the thermally induced precipitation of $TiCl_4$ in hydrochloric acid at a concentration of 3 mol L^{-1} according to a previously described method [41]. Typically, 9 mL of pure $TiCl_4$ was added dropwise in 450 mL of a 3 mol L^{-1} hydrochloric acid solution under vigorous magnetic stirring and cooled down in an ice bath. The obtained transparent solution was placed in a closed vessel in an oven at 100 °C for 24 h. An additional peptization step is performed in a 3 mol L^{-1} nitric acid solution to separate the supernatant solution that contains only brookite nanoparticles from the precipitate containing mainly the rutile phase.

Co-hydrolysis of $TiCl_3$ and $TiCl_4$ (B-Ti(III)/(IV)) [42] An equimolar solution of $TiCl_3$ and $TiCl_4$ (0.1 mol L^{-1}) was prepared and the pH was adjusted to 4.5 with NaOH solution of 5 mol L^{-1} under magnetic stirring. The suspension was aged 1 week at 60 °C without stirring. The particles were flocculated by increasing the pH up to 6 with NaOH (close to the isoelectric point).

The reference anatase and rutile nanoparticles were synthesized as follow:

Thermohydrolysis of $TiCl_4$ in the presence of glutamic acid (A). This synthesis was adapted from a previously reported procedure [43, 44]. A stock solution with Ti(IV) concentration of 1 mol L^{-1} was prepared by dilution of $TiCl_4$ in 3 mol L^{-1} HCl solution. In addition to the 30 mL of Ti(IV) stock solution, a 1.98 g amount of glutamic acid (GA) was introduced at room temperature under stirring into 100 mL of Milli-Q water in order to obtain a [GA]/[Ti] molar ratio of 0.5. Then, the pH of the clear solution was set to 4 by addition of sodium hydroxide solution under stirring, and the sample volume was completed to 300 mL with water. The suspension was aged at 120 °C in an oven for 48 h.

Thermohydrolysis of $TiCl_4$ in acidic medium (R) TiO_2 rutile particles were obtained through the thermally induced precipitation of $TiCl_4$ in hydrochloric acid at a concentration of 1 mol L^{-1} according to a previously described method [41]. Typically, 4.2 mL of pure $TiCl_4$ was added dropwise in 250 mL of a 1 mol L^{-1} hydrochloric acid solution under stirring and cooled down in an ice bath. The obtained transparent solution was placed in a round-bottom flask and heated under reflux of the solvent for 1 week. A precipitate appeared after few minutes of reflux.

After all the syntheses, the solids were separate from the reacting medium by centrifugation (29220 g for 20 min) and washed according to a standard procedure: three washing steps H_2O/HNO_3 3 mol L^{-1}/H_2O where the particles are suspended in the washing solution by ultrasonication and then separated by centrifugation.

Characterization

The structure and size of the nanoparticles were determined using a precise deconvolution of the corresponding X-ray diffraction (XRD) patterns. Bragg–Brentano XRD measurements were performed on a Brucker D8 diffractometer using filtered Cu K_α radiation over a 2θ range from 5° to 80° with a step size of 0.033° and a counting time of 300 s per step. The size of the particles in a defined direction, D_{hkl}, was calculated by applying the Scherrer formula, $D_{hkl} = 0.9\lambda/B_{hkl} \cos\theta$, to the line width at half maximum, B_{hkl}, corrected for the instrument broadening assuming a Gaussian profile. It was also assumed that line broadening is mainly due to the particle size effect.

UV–visible diffuse reflectance spectra (DRS) of the different sample powders were recorded on a Agilent Cary 5000 spectrometer with integrating sphere from 300 to 800 nm.

Transmission electron microscopy (TEM) images were noted on a FEI Tecnai Spirit G2 instrument at an acceleration voltage of 120.0 kV. The nanoparticles were ultrasonicated in water and dispersed on carbon-covered Cu grids. High-resolution TEM (HRTEM) was performed at 200 kV using a Jeol-Jem 2011HR apparatus (LaB_6). At least 100 particles were measured on TEM images to determine their size.

Raman spectra were recorded at room temperature in the 100–700 cm^{-1} range using the Raman Analyzer RXN1 microprobe (Kaiser Optical Systems, Inc.) equipped with a 785-nm high-powered near-IR diode laser for excitation and a Leica microscope as microprobe.

The specific surface area measurements were carried out by N_2 adsorption isotherm at 77 K using a Belsorb Max instrument. Prior to measurements, TiO_2 powders were degassed under a primary vacuum at 150 °C and flowing nitrogen gas overnight using a Belprep II instrument in order to remove any adsorbed organic compounds and water molecules. The BET method was applied to determine the specific surface area.

The charge carrier lifetimes in TiO_2 after UV irradiation were determined by microwave absorption experiments using the TRMC method. Measurements were carried out as previously described [45]. The microwaves were generated by means of a Gunn diode in the K_α band (28–38 GHz). All experiments were carried out at the highest microwave power (at 31.4 GHz). The reflected microwaves were detected by a Schottky diode. The emitted signal was amplified and displayed on a digitizer. The pulsed light source was an OPO laser (EKSPLA, NT342B) tunable from 225 to 2000 nm. It delivers 8-ns FWMH pulses with a frequency of 10 Hz. The measurements were realized under UV light (355 nm). The maximum light energy received by the sample was 1.5 $mJ.cm^{-2}$.

Photocatalytic activity test

Photoreactor and light source A cylindrical batch photoreactor made of Pyrex with a bottom optical window of ca. 5 cm diameter open to air was used for the different experiments. Irradiation was provided by a high-pressure mercury lamp (Philips HPK 125 W) which provides maximum energy at 365 nm. An optical filter Corning 0.52 was installed to cutoff wavelength below 340 nm. The circulating-water cell (thickness 2.2 cm) was used to remove IR radiation, thus preventing any heating of the suspension. The radiant flux was measured with a VLX-3 W radiometer with a CX-365 detector (UV-A). The distance which separates the photoreactor from the water cell is regulated in order to preserve the radiant flux constant at 4.5 $mW.cm^{-2}$ for all photocatalytic tests. At different times of photoreaction (10 min steps in the first hour), samples were taken with 1-mL syringe and filtered using a 0.45-μm Millipore filter to remove TiO_2 particles before analysis.

Procedure A volume of 100 mL of formic acid (FA) or phenol with a concentration of 1086 μmol L^{-1} of carbon was introduced in photoreactor with 50 mg of TiO_2 photocatalysts was mechanically stirred (Mixel TT, 500 $tr.min^{-1}$) under dark condition during 30 min. This time was necessary to reach the adsorption–desorption equilibrium. The photocatalytic degradations were carried out at room temperature, under the same stirring condition and at pH = 3.5 for FA and 6 for phenol.

Analytical determination The concentrations of FA and phenol were determined using HPLC analysis. For phenol the HPLC analyses were performed using VARIAN system with a diode array and on a 125 mm × 4 mm C18 reverse-phase column (Agilent technology). The mobile phase composition was methanol and water acidified with phosphoric acid (pH 3.0) at a volume ratio 5:95. For FA the HPLC analyses were performed using VARIAN system with single wavelength UV–Vis detector and a 300 mm ×

7.8 mm carbohydrate analysis column (COREGEL-87H3) was used. The mobile phase was H_2SO_4 solution (5.10^{-3} mol L^{-1}) and the flow rate was set at 0.7 mL min^{-1}. The detection wavelength was set at 210 nm.

Results and discussion

Characterization of the TiO_2 nanoparticles

The below-described brookite syntheses differ in terms of titanium precursor, acidity of the reacting medium, presence of organic additives, temperature, and duration of the thermohydrolysis. The experimental conditions were selected from the literature and from our own expertise to ensure a good purity of brookite. The syntheses indeed all lead to the same pure crystalline structure as observed in the X-ray diffraction patterns reported in Fig. 2. All the diffraction lines observed for the B samples could be attributed to brookite according to the PDF card 29-1360 (orthorhombic *Pbca* space group). The diffraction lines of B-lactate and B-NaOH samples are significantly thinner than the other two samples indicating larger crystallites. A mean crystallite size of brookite particles was determined from the diffraction patterns using Scherrer equation on five different lines ((121), (221), (032), (231) and (132)). Results are reported in Table 1. The diffraction patterns of pure anatase and rutile samples as well as the commercial TiO_2 P25 (Evonik) powder are also reported in Fig. 2.

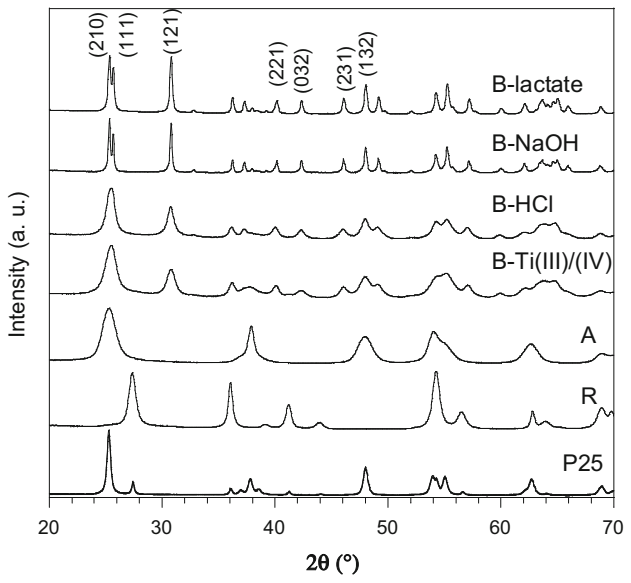

Figure 2 X-ray diffraction patterns of the four brookite samples and anatase, rutile and P25 references. Brookite, anatase, and rutile peaks could be indexed according to 00-29-1360, 00-21-1272 and 00-21-1276 PDF cards respectivly.

The diffraction lines of the pure phase samples could be indexed according to the 00-21-1272 and 00-21-1276 PDF files, respectively. Peaks of both structures could be found in the TiO_2 P25 powder as this material is a composite of 87% anatase phase and 13% of rutile phase. A closer look to anatase and brookite peaks positions shows that a brookite sample may contain few percent of anatase phase without changing significantly the diffraction pattern as most of the anatase diffraction lines can be hidden by brookite ones. That is why a more accurate Raman spectroscopy study is mandatory to confirm that phase pure brookite has really been prepared. The Raman spectra of the four brookite samples are reported in Fig. 3 and those of anatase, rutile, and P25 samples are reported in Online Resource-1. Four modes are Raman active in the brookite structure resulting in 15 vibration bands in the 100 to 700 cm^{-1} range which are A_{1g} (155, 194, 247, 412, and 636 cm^{-1}), B_{1g} (213, 322, and 501 cm^{-1}), B_{2g} (366, 395,460 and 583 cm^{-1}), and B_{3g} (172, 287, and 545 cm^{-1}) [46]. All these bands can be found in the four spectra with the noticeable specificity of B-Ti(III)/(IV) spectrum that presents a particularly feeble A_{1g} band at 155 cm^{-1}. This may be due to a lower crystalline quality in agreement with the small crystallite size. In addition to those bands no shouldering could be observed at 442 and 516 cm^{-1} that are specific to rutile and anatase structures, respectively [47]. The Raman study confirms then that all the brookite samples are pure phases.

The four brookite materials prepared significantly differ in their particles size and morphology as shown in the TEM and HRTEM images reported in Fig. 4. The first set of experimental B-lactate conditions gave monocrystalline nanoparticles with a rather narrow size distribution around 50 nm. The specificity of our adapted procedure compared to the original work is that particles obtained are well facetted isotropic particles (Fig. 4a), whereas Kandiel et al. protocol gave rods [26]. The morphology is closer to that of Lin et al. that obtained thick platelets from the same lactate complex [21]. The relative transparency of the particle is in agreement with

Table 1 Structural, microstructural, electronic, optical, and photocatalytic properties of various TiO_2 brookite compounds along with anatase, rutile, and P25 references

Sample	Crystallites size from XRD (nm)	Particles size from TEM (nm) (± 5%)	Specific surface ($m^2.g^{-1}$) (± 2%)	Band gap (ev) (± 0.02)	I_{40ns}/I_{max}	Initial disappearance rate FA (μmol/L/min)	Initial disappearance rate phenol (μmol/L/min)
B-lactate	37 ± 2	53×43	28	3.24	0.60	7.2	1
B-NaOH	46 ± 2	500×200[a]	10	3.32	0.67	3.8	0.4
B-HCl	12 ± 1	71×48[a]	150	3.27	0.27	8.6	0.4
B-Ti(III)/(IV)	10 ± 1	17×8	185	3.22	0.50	9.1	1.2
A	12 ± 1	14×6	215	3.10	0.41	7.4	1.1
R	20 ± 1	95×17	46	2.95	/	4.7	0.6
P25	20/30 (A/R)	25	50	n. c.	0.67	12.2	1.2

[a]Dimensions of aggregates

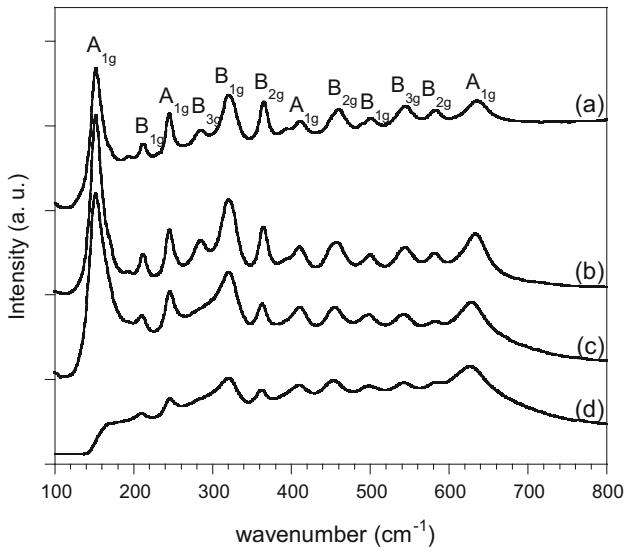

Figure 3 Raman spectra of the (a) B-lactate, (b) B-NaOH, (c) B-HCl, and (d) B-Ti(III)/(IV) brookite samples.

platelet morphology and the lattice planes observed in the HRTEM image also confirms that similarity.

The second preparation mode (B-NaOH) consists in an hydrothermal aging of a titanate colloidal solution obtained in mild alkaline conditions. After 1 day, at 200 °C bundles of brookite rods are obtained (Fig. 4c). The rods are about 50 nm thick and between 200 and 500 nm long. On HRTEM images (Fig. 4d), the lattice fringes observed are attributed to (111) or (210) planes which are very close in distance. These lattice fringes are observed in a detailed study of brookite platelets proposed by Lin et al. [21] and by Zhao et al. [22] for brookite rods presenting the same growth orientation. Brookite particles formed in highly acidic conditions B-HCl are rectangular platelets (Fig. 4e) of about 70 nm long and 50 nm large. They seem to consist of smaller subunits that have aggregated to form these platelets. The HRTEM image (Fig. 4f) of B-HCl show {210} lattice fringes on the whole particle indicating an oriented attachment of the initial crystallites that are more in the 10-nm size range to form larger rectangle platelets. This morphology is in agreement with the one described the original publication [41]. The particles of the last sample B-Ti(III)/(IV) are also rather small and present a slight anisotropy with a mean length of 17 nm and a width of 8 nm (Fig. 4g). HRTEM images (Fig. 4h) show the same {210} lattice fringes along the main axis and consequently the same elongation direction as in the B-NaOH sample. The TEM images of the anatase and rutile reference samples are reported in Online Resource-2. As previously described [41, 43], anatase particles present an elongated octahedral morphology with {101} exposed surfaces while rutile rods are elongated in the [001] direction with {110} as mainly exposed surfaces. As for TiO_2 P25, isotropic particles with mean particles size of 25 nm are observed.

Two other significant characteristics of photocatalytic materials were determined on the different brookite samples and on the references: specific

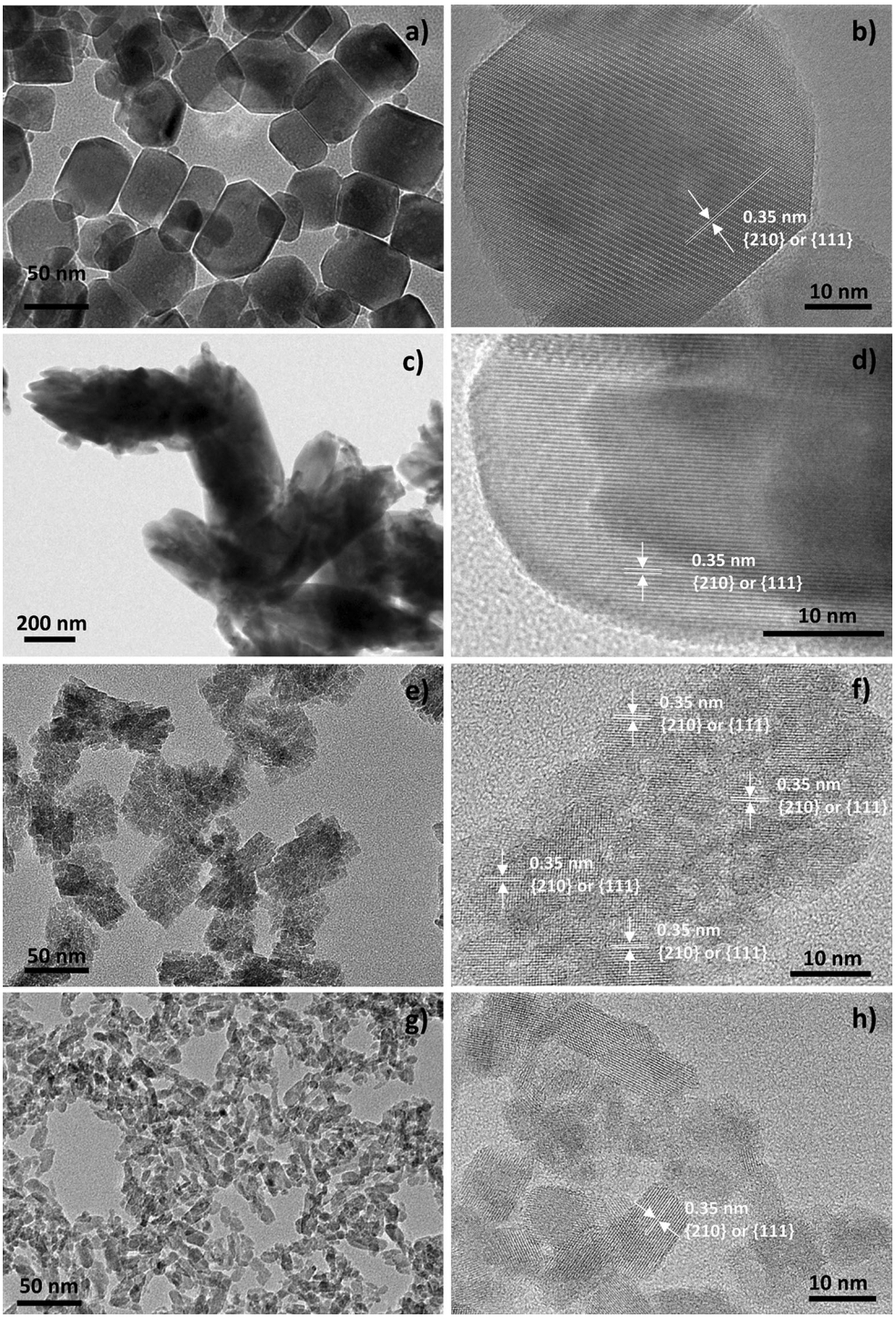

Figure 4 TEM and HRTEM images of the four different brookite samples: **a**–**b** B-lactate, **c**–**d** B-NaOH, **e**–**f** B-HCl, **g**–**h** B-Ti(III)/(IV).

surface and optical bandgap. These values are reported in Table 1. For a crystalline semiconductor, the optical absorption near the band edge follows the formula $\alpha h\nu = A(h\nu - E_g)^{n/2}$ where α, h, ν, E_g and A correspond to absorption coefficient, Planck constant, light frequency, band gap, and a constant, respectively. The last parameter n depends on the characteristics of the transition in a semiconductor, for a direct transition, $n = 1$, whereas for an indirect transition, $n = 4$. The bandgap calculations for brookite were done assuming an indirect bandgap. (This point is still controversial; for more details see [10].)

Hence, the band gap energy is estimated on the plot $(Ahv)^{1/2} = f(hv)$ by the intercept of the tangent to the plot with abscissa. The corresponding plots are reported in Online Resource-3 for all brookite samples. The characteristics of the three reference samples TiO_2 anatase, TiO_2 rutile, and the commercial TiO_2 P25 are also reported in Table 1.

Photocatalytic activity

The photocatalytic activities of the different materials have been studied using two model pollutants, formic acid (FA), and phenol. Their initial abatement rate corresponding to triplicate experiments are given in Table 1 and represented in Fig. 5 (raw data are reported in online resources 4). In the case of FA, it is a true degradation rate as it directly forms water and carbon dioxide. The phenol may be degraded in several intermediates before complete mineralization, and for the sake of conciseness, we chose to focus on its abatement to compare the different materials. Whatever the pollutant, we first notice that TiO_2 P25 has always the higher activity. Then the brookite sample B-Ti(III)/(IV) is the second best sample, while B-NaOH is the less efficient photocatalyst. More in details, two of the brookite samples (B-lactate and B-Ti(III)/(IV)) have a systematically higher activity than anatase in FA degradation and very similar in phenol abatement. Between the different brookite samples, only B-NaOH presents really low photocatalytic activity that may be attributed to its very low specific surface. Surprisingly, the B-HCl sample gives good results in FA degradation, while the abatement rate is quite low in the case of phenol. This significant difference when compared to other materials may hardly be explained. We may just remind that FA degradation generally involves more surface–pollutant interactions and hole transfers, while first phenol degradation step is an oxidation by free radicals in solution [34]. Consequently, an explanation to observed differences in activity may be attributed to a lower production of hydroxyl radicals on the exposed surfaces of the B-HCl sample [21].

When plotting the degradation efficiency as a function of specific surface in Fig. 6, a general trend observed is a global increase in the activity with specific surface. In addition to the case of B-HCl on phenol abatement discussed above, the two exceptions are TiO_2 P25 and the B-lactate sample. Indeed, this brookite sample presents good activity for a relatively low specific surface of 28 $m^2\ g^{-1}$.

The first key result of this study is that selected brookite systems can be at least as efficient as good anatase photocatalysts and close to the TiO_2 P25 reference. The corollary to this finding, as for anatase, is that a selection among different brookite nanomaterials must be done. We have chosen to study the abatement of FA and phenol in water for reasons discussed in a previous paper [44]. Some studies in the literature on methyl orange and As(III) oxidation have also shown the good efficiency of selected brookite samples [48]. A second important point is that a large specific surface generally leads to an increased photoactivity. The two materials P25 and

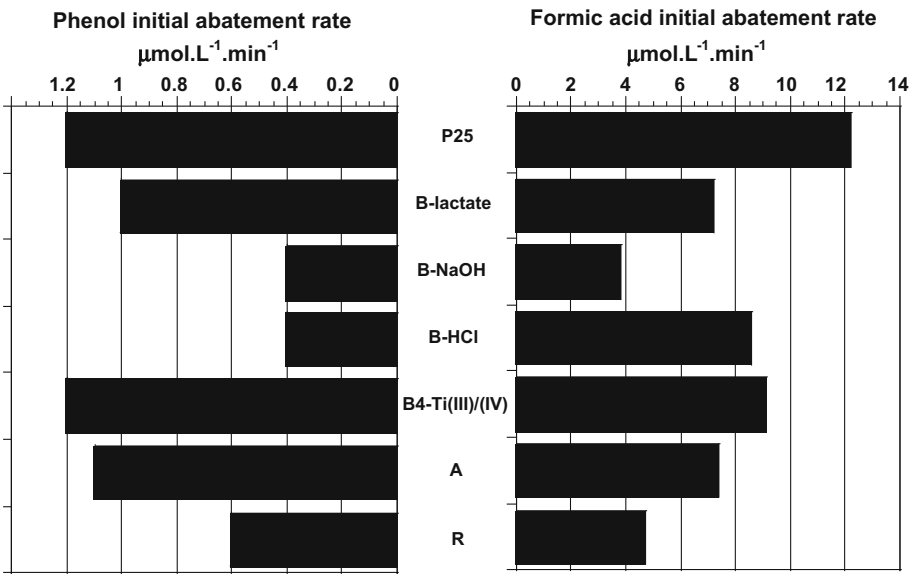

Figure 5 Initial abatement rate of phenol and formic acid in the presence of the various brookite sample and anatase, rutile, and P25 references.

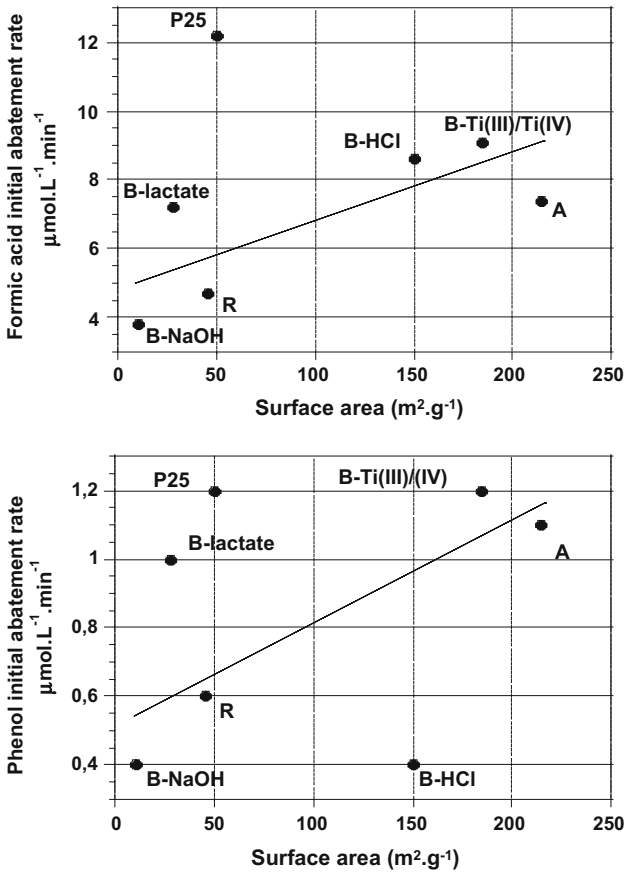

Figure 6 Initial abatement rate of formic acid and phenol as function of specific surface. Dotted lines are just guidelines for the eyes.

B-lactate differ from that general trend with their good photocatalytic activity despite a low specific surface. The efficiency of the first one is still matter of debate: good crystallinity, good charge-carrier separation in the composite, or more active surface hydroxyl groups [49, 50]. The good activity of the B-lactate brookite sample may come from its good crystallinity or from the nature of exposed faces as stressed in the literature [21]. On the contrary, the negative deviation to the above-mentioned rule on specific surface is the B-HCl sample and only for phenol abatement. This means that charge carriers are efficiently trapped close to the surface for direct transfer to adsorbed pollutants but that the exposed surfaces should be less efficient in active radical production for indirect degradation.

These two brookite samples B-lactate and B-HCl clearly demonstrate that, in addition to the size and the associated specific surface, the crystalline quality and the exposed faces are involved in the photocatalytic efficiency of TiO_2 brookite materials. In order to focus a little more on bulk properties, we have studied the charge carrier mobility through TRMC measurements.

Photogenerated charge carriers

TRMC is a valuable technique to study charge-carrier generation in photocatalysts, their lifetime, and mobility. More specifically, for n-type semiconductors such as titanium dioxide, the observed charge carriers in TRMC are the electrons because their mobility is much higher than that of the holes [51]. Moreover, for low-mobility semiconductors such as TiO_2, the microwave absorbance is due to free mobile electrons in the conduction band and in shallow traps. The signals reported in Fig. 7 present two time domains: the intensity increases just after the laser pulse during few nanoseconds and its decay over several microseconds. The maximum intensity reached can be, in a first approach, correlated with the amount of photogenerated free charge carriers in the bulk. It is then possible to compare the three polymorphs of TiO_2 and P25 using that value.

The maximum intensity order is then P25 > B-lactate = B-NaOH > A > B-HCl ~ B-Ti(III)/(IV) ~ R. The significantly good value observed for the commercial photocatalyst was already discussed in the literature [52] and is attributed to a lower trap density rather than the presence of rutile in addition to anatase. In the same publication, Nakajima et al. also show that the maximum signal intensity is proportional to particles diameter, i.e., higher intensity for bigger particles. However, most of the commercial samples studied in this article contain only or mostly anatase, the rutile, and P25 sample studied which were discarded from this trend. In our study, P25 sample again does not follow the correlation of signal intensity with crystallites size and this trend could not be applied to pure samples with different structure. Indeed, anatase particles of 12 nm gave more intense signal than brookite particles of the same size or bigger rutile particles (d ~ 20 nm). Among the brookite samples, the trend is roughly respected with the bigger crystallites B-lactate and B-NaOH presenting a more intense signal than B-HCl and B-Ti(III)/(IV). The significantly low rutile signal was already observed in previous studies [53] and is attributed to a fast charge recombination that occurs just after the pulse. A theoretical approach of electron

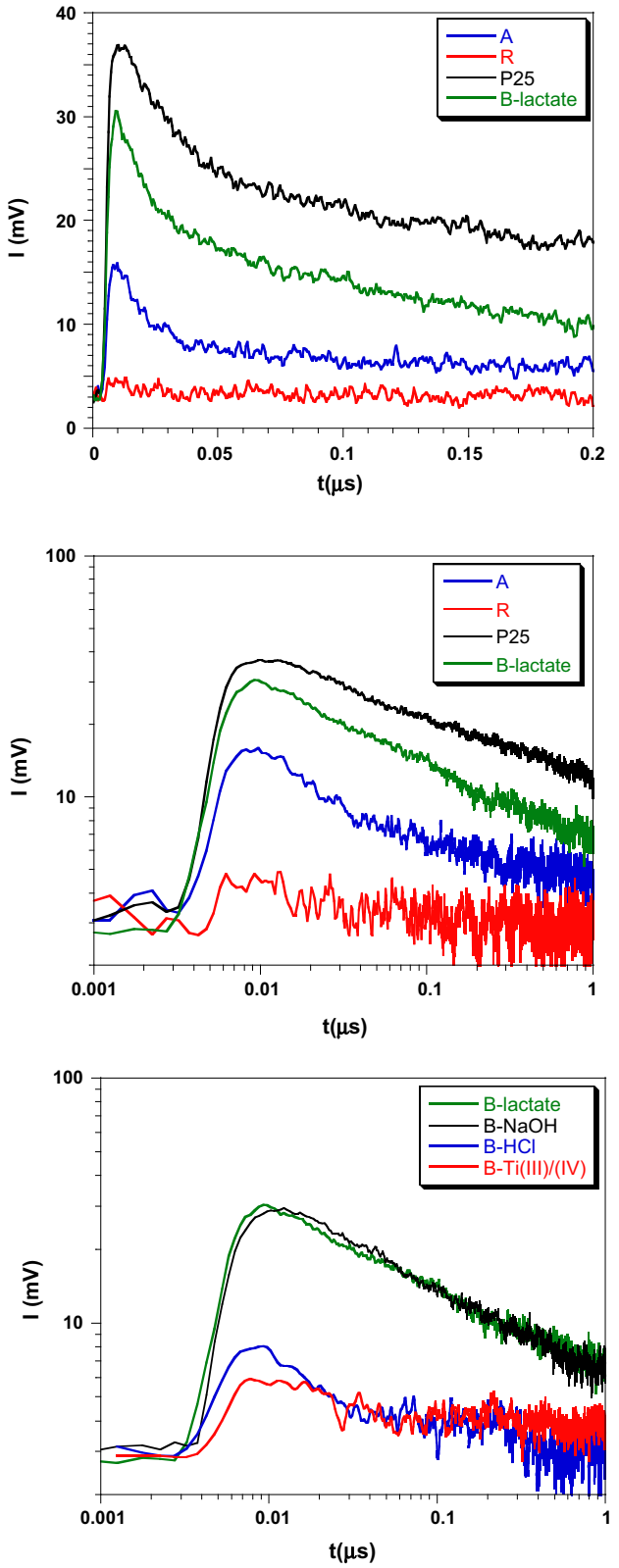

Figure 7 TRMC intensity signal decays for different TiO_2 polymorphs in lin. lin. (top) or log. log. graph (middle) and for the brookite samples (bottom).

mobility in anatase and rutile [12] pointed out that the electron effective mass is 17 times higher in rutile than in anatase. This may also account for the very low rutile signal.

The signal decay phase is generally split in two regimes depending on the recombination mechanism. Fast recombination occurring in the first 40 ns is generally attributed to 'free' holes/electrons recombination while, at longer time, recombination involves trapped species. In the double-logarithmic plots of Fig. 7, this corresponds roughly to two slopes before and after 40 ns. For the first part we may then use the I_{40ns}/I_{max} ratio to estimate the importance of the first recombination mechanism. The values are reported in Table 1 except for rutile sample that present an excessive signal to noise ratio. Again P25 presents interestingly few fast recombinations that allow an efficient use of photogenerated charge carriers. For the other samples including anatase reference, lower recombination is observed for bigger crystallites. Indeed, $I_{40ns}/I_{max} > 0.6$ for B-lactate and B-NaOH particles ($d \sim 40$ nm), whereas is it ≤ 0.5 for B-HCl, B-Ti(III)/(IV) and A ($d \sim 10$ nm). Moreover, in that second set of particles, the B-Ti(III)/(IV) sample presents lower recombination rates than B-HCl and A. The second part of the signal decay is roughly the same for all samples except P25, A and B-Ti(III)/(IV) that present a lower decay. The lower decay and hence the higher amount of long-living photogenerated charge carriers may explain the significantly good photocatalytic results of B-Ti(III)/(IV) for phenol abatement where long-lived surface trapped holes are necessary to create hydroxyl radicals.

The correspondence between TRMC results and photocatalytic efficiency is not straightforward. High maximum signal intensity is not sufficient for good degradation results of the photocatalyst as demonstrated with the B-NaOH sample. However, the very low specific surface of B-NaOH is the limiting parameter for its photocatalytic activity. The differences in TRMC signal of B-HCl and B-Ti(III)/(IV) may provide keys for the differences in photocatalytic activity. The two samples display rather close maximal signal intensity (B-HCl is even slightly higher), but with longer charge-carrier lifetimes, B-Ti(III)/(IV) may be more active especially for degradation processes that will involve hydroxyl radicals generated from sub-surface-trapped holes.

Conclusions

Four different brookite samples are successfully prepared varying experimental conditions such as titanium source, pH of the reacting medium use of organic additive. X-ray diffraction and Raman spectroscopy were combined to ensure the purity of the obtained product. Their optical characterization gave very close bandgap values around 3.25 eV, while other characteristics were very different with a crystallite size from 10 to 40 nm and a specific surface form 10 to 185 $m^2\ g^{-1}$. The photocatalytic degradation test on FA for the four brookite samples revealed that half of them are more efficient than the rutile and anatase references [44]. These values are still lower than TiO_2 P25. This is not the case with phenol abatement where one brookite sample is competitive with the commercial photocatalyst P25. The best brookite sample B-Ti(III)/(IV) exhibits the highest specific surface and it exhibits a good crystalline quality. This sample surprisingly presents a low TRMC signal intensity but a slow signal decay that may be beneficial for active radicals in solution. However, the high specific surface criterion for good efficiency is not always respected as the second best brookite sample for phenol abatement B-lactate presents a specific surface seven times smaller than the best one. This brookite B-lactate sample gave the best TRMC signal intensity among pure phase samples indicating a more efficient photon harvesting. Then its surface is appropriate for high active radical generation such as hydroxides while it is not enough for formic acid adsorption. This study clearly demonstrates that one model pollutant is not enough to classify photocatalyst. It is now clear that the TiO_2 brookite phase may be at least as efficient as the anatase polymorph for photocatalytic depollution then it may be the same other light driven properties as it is emerging in the literature.

Supporting information available

Raman spectra of the anatase, rutile, and TiO_2 P25 samples, TEM images of the anatase, rutile, and TiO_2 P25 samples.

Acknowledgements

The authors thank J.-M. Krafft (LRS, UPMC, France) for its precious help in Raman spectra acquisition and S. Casale (LRS, UPMC, France) for the HRTEM analyses. Funding: This work was supported by the French Agence Nationale de la Recherche (ANR) through the PhotoNorm project.

Funding

This study was funded by the Agence 678Nationale de la Recherche (ANR Photonorm).

Compliance with ethical standards

Conflict of interest The authors declare that they have no conflict of interest.

Electronic supplementary material: The online version of this article (https://doi.org/10.1007/s10853-018-2924-x) contains supplementary material, which is available to authorized users.

References

[1] Weir A, Westerhoff P, Fabricius L, Hristovski K, von Goetz N (2012) Titanium dioxide nanoparticles in food and personal care products. Environ Sci Technol 46:2242–2250

[2] Fujishima A, Rao TN, Tryk DA (2000) Titanium dioxide photocatalysis. J Photochem Photobiol C 1:1–21

[3] Bonhôte P, Moser J-E, Humphry-Baker R et al (1999) Long-lived photoinduced charge separation and redox-type photochromism on mesoporous oxide films sensitized by molecular dyads. J Am Chem Soc 121:1324–1336

[4] Lin H-M, Keng C-H, Tung C-Y (1997) Gas-sensing properties of nanocrystalline TiO2. Nanostruct Mater 9:747–750

[5] Croce F, Appetecchi GB, Persi L, Scrosati B (1998) Nanocomposite polymer electrolytes for lithium batteries. Nature 394:456–458

[6] Baudrin E, Cassaignon S, Koesch M, Jolivet JP, Dupont L, Tarascon JM (2007) Structural evolution during the reaction of Li with nano-sized rutile type TiO2 at room temperature. Electrochem Commun 9:337–342

[7] Magne C, Cassaignon S, Lancel G, Pauporte T (2011) Brookite TiO(2) nanoparticle films for dye-sensitized solar cells. ChemPhysChem 12:2461–2467

[8] Reisch M (2001) Paints and coatings. Chem Eng News 79:23–28

[9] Henderson MA (2011) A surface science perspective on TiO(2) photocatalysis. Surf Sci Rep 66:185–297

[10] Di Paola A, Bellardita M, Palmisano L (2013) Brookite, the Least Known TiO2 photocatalyst. Catalysts 3:36–73

[11] Di Paola A, Bellardita M, Palmisano L, Barbierikova Z, Brezova V (2014) Influence of crystallinity and OH surface density on the photocatalytic activity of TiO2 powders, J. Photochem Photobiol A 273:59–67

[12] Le Bahers T, Rérat M, Sautet P (2014) Semiconductors used in photovoltaic and photocatalytic devices: assessing fundamental properties from DFT. J Phys Chem C 118:5997–6008

[13] Dou M, Persson C (2013) Comparative study of rutile and anatase SnO2 and TiO2: band-edge structures, dielectric functions, and polaron effects. J Appl Phys 113:083703

[14] Ozawa K, Emori M, Yamamoto S et al (2014) Electron-hole recombination time at TiO2 single-crystal surfaces: influence of surface band bending. J Phys Chem Lett 5:1953–1957

[15] Mino L, Spoto G, Bordiga S, Zecchina A (2012) Particles morphology and surface properties as investigated by HRTEM, FTIR, and periodic DFT calculations: from pyrogenic TiO2 (P25) to nanoanatase. J Phys Chem C 116:17008–17018

[16] Odling G, Robertson N (2015) Why is anatase a better photocatalyst than rutile? The importance of free hydroxyl radicals. ChemSusChem 8:1838–1840

[17] Lin H, Huang CP, Li W, Ni C, Shah SI, Tseng Y-H (2006) Size dependency of nanocrystalline TiO2 on its optical property and photocatalytic reactivity exemplified by 2-chlorophenol. Appl Catal B 68:1–11

[18] Tachikawa T, Yamashita S, Majima T (2011) Evidence for crystal-face-dependent TIO_2 photocatalysis from single-molecule imaging and kinetic analysis. J Am Chem Soc 133:7197–7204

[19] Liu S, Yu J, Jaroniec M (2011) Anatase TiO_2 with dominant high-energy 001 Facets: synthesis, properties, and applications. Chem Mater 23:4085–4093

[20] Ohno Y, Tomita K, Komatsubara Y et al (2011) Pseudo-cube shaped brookite (TiO_2) nanocrystals synthesized by an oleate-modified hydrothermal growth method. Cryst Growth Des 11:4831–4836

[21] Lin H, Li L, Zhao M et al (2012) Synthesis of high-quality brookite TiO_2 Single-crystalline nanosheets with specific facets exposed: tuning catalysts from inert to highly reactive. J Am Chem Soc 134:8328–8331

[22] Zhao M, Xu H, Chen H et al (2015) Photocatalytic reactivity of 121 and 211 facets of brookite TiO_2 crystals. J Mater Chem A 3:2331–2337

[23] Cargnello M, Montini T, Smolin SY et al (2016) Engineering titania nanostructure to tune and improve its photocatalytic activity. Proc Natl Acad Sci USA 113:3966–3971

[24] Pourjafari D, Reyes-Coronado D, Vega-Poot A et al (2018) Brookite-based dye-sensitized solar cells: influence of morphology and surface chemistry on cell performance. J Phys Chem C 122:14277–14288

[25] Choi M, Lim J, Baek M, Choi W, Kim W, Yong K (2017) Investigating the unrevealed photocatalytic activity and stability of nanostructured brookite TiO2 film as an environmental photocatalyst. ACS Appl Mater Interfaces 9:16252–16260

[26] Kandiel TA, Feldhoff A, Robben L, Dillert R, Bahnemann DW (2010) Tailored titanium dioxide nanomaterials: anatase nanoparticles and brookite nanorods as highly active photocatalysts. Chem Mater 22:2050–2060

[27] Ismail AA, Kandiel TA, Bahnemann DW (2010) Novel (and better?) titania-based photocatalysts: brookite nanorods and mesoporous structures. J Photochem. Photobiol A 216:183–193

[28] Kobayashi M, Tomita K, Petrykin V et al (2007) Hydrothermal synthesis of nanosized titania photocatalysts using novel water-soluble titanium complexes. Solid State Phenom 124–126:723–726

[29] Stengl V, Bakardjieva S, Murafa N, Subrt J, Mest'ankova H, Jirkovsky J (2007) Preparation, characterization and photocatalytic activity of optically transparent titanium dioxide particles. Mater Chem Phys 105:38–46

[30] Zhao B, Chen F, Huang Q, Zhang J (2009) Brookite TiO2 nanoflowers. Chem Commun 34:5115–5117

[31] Vequizo JJM, Matsunaga H, Ishiku T, Kamimura S, Ohno T, Yamakata A (2017) Trapping-induced enhancement of photocatalytic activity on brookite TiO2 powders: comparison with anatase and rutile TIO2 powders. ACS Catal 7:2644–2651

[32] Monai M, Montini T, Fornasiero P (2017) Brookite: nothing new under the sun? Catalysts 7:304

[33] Yang Z, Wang B, Cui H, An H, Pan Y, Zhai J (2015) Synthesis of crystal-controlled TiO2 nanorods by a hydrothermal method: rutile and brookite as highly active photocatalysts. J Phys Chem C 119:16905–16912

[34] Montoya JF, Velasquez JA, Salvador P (2009) The direct-indirect kinetic model in photocatalysis: a reanalysis of phenol and formic acid degradation rate dependence on photon flow and concentration in TiO2 aqueous dispersions. Appl Catal B 88:50–58

[35] Turki A, Guillard C, Dappozze F, Ksibi Z, Berhault G, Kochkar H (2015) Phenol photocatalytic degradation over anisotropic TiO2 nanomaterials: kinetic study, adsorption

isotherms and formal mechanisms. Appl Catal B 163:404–414

[36] Turki A, Guillard C, Dappozze F, Berhault G, Ksibi Z, Kochkar H (2014) Design of TiO2 nanomaterials for the photodegradation of formic acid—adsorption isotherms and kinetics study. J Photochem Photobiol 279:8–16

[37] Quang Duc T, Thi Hang L, Huu Thu H (2017) Amino acid-assisted controlling the shapes of rutile, brookite for enhanced photocatalytic CO2 reduction. CrystEngComm 19:4519–4527

[38] Pottier A, Chanéac C, Tronc E, Mazerolles L, Jolivet J-P (2001) Synthesis of brookite TiO2 nanoparticles by thermolysis of TiCl4 in strongly acidic aqueous media. J Mater Chem 11:1116–1121

[39] Kakihana M, Kobayashi M, Tomita K, Petrykin V (2010) Application of water-soluble titanium complexes as precursors for synthesis of titanium-containing oxides via aqueous solution processes. Bull Chem Soc Jpn 83:1285–1308

[40] Nagase T, Ebina T, Iwasaki T, Hayashi K, Onodera Y, Chatterjee M (1999) Hydrothermal synthesis of brookite. Chem Lett 28:911–912

[41] Pottier A, Chanéac C, Tronc E, Mazerolles L, Jolivet J-P (2001) Synthesis of brookite TiO2 nanoparticles by thermolysis of TiCl4 in strongly acidic aqueous media. J Mater Chem 11:1116–1121

[42] Perego C, Clemençon I, Rebours B, et al (2009) Thermal stability of brookite—TiO2 nanoparticles with controlled size and shape: in situ studies by XRD. In: Mater. Res. Soc. Symp. Proc. 1146: NN04-02

[43] Durupthy O, Bill J, Aldinger F (2007) Bioinspired synthesis of crystalline TiO2: effect of amino acids on nanoparticles structure and shape. Cryst Growth Des 7:2696–2704

[44] Pigeot-Rémy S, Dufour F, Herissan A et al (2017) Bipyramidal anatase TiO2 nanoparticles, a highly efficient photocatalyst? Towards a better understanding of the reactivity. Appl Catal B 203:324–334

[45] Emilio CA, Litter MI, Kunst M, Bouchard M, Colbeau-justin C (2006) Phenol photodegradation on platinized-TiO 2 photocatalysts related to charge-carrier dynamics. Langmuir 22:4943–4950

[46] Tompsett GA, Bowmaker GA, Cooney RP, Metson JB, Rodgers KA, Seakins JM (1995) The Raman spectrum of brookite, TiO2 (Pbca, Z = 8). J Raman Spectrosc 26:57–62

[47] Tran HTT, Kosslick H, Ibad MF et al (2016) Photocatalytic performance of highly active brookite in the degradation of hazardous organic compounds compared to anatase and rutile. Appl Catal B 200:647–658

[48] Lopez-Munoz MJ, Revilla A, Alcalde G (2015) Brookite TiO2-based materials: synthesis and photocatalytic performance in oxidation of methyl orange and As(III) in aqueous suspensions. Catal Today 240:138–145

[49] Deiana C, Fois E, Coluccia S, Martra G (2010) Surface structure of TiO2 P25 nanoparticles: infrared study of hydroxy groups on coordinative defect sites. J Phys Chem C 114:21531–21538

[50] Hurum DC, Agrios AG, Gray KA, Rajh T, Thurnauer MC (2003) Explaining the enhanced photocatalytic activity of degussa P25 mixed-phase TiO2 using EPR. J Phys Chem B 107:4545–4549

[51] Kroeze JE, Savenije TJ, Warman JM (2004) Electrodeless determination of the trap density, decay kinetics, and charge separation efficiency of dye-sensitized nanocrystalline TiO2. J Am Chem Soc 126:7608–7618

[52] Nakajima S, Katoh R (2015) Time-resolved microwave conductivity study of charge carrier dynamics in commercially available TiO2 photocatalysts. J Mater Chem A 3:15466–15472

[53] Kolen'ko YV, Churagulov BR, Kunst M, Mazerolles L, Colbeau-Justin C (2004) Photocatalytic properties of titania powders prepared by hydrothermal method. Appl Catal B 54:51–58